



Title	Histopathological changes in tear-secreting tissues and cornea in a mouse model of autoimmune disease
Author(s)	Masaya, Hiraishi; Md Abdul, Masum; Takashi, Namba; Otani, Yuki; Elewa, Yaser H. A.; Ichii, Osamu; Kon, Yasuhiro
Citation	Experimental Biology and Medicine, 245(12), 999-1008 <a href="https://doi.org/10.1177/1535370220928275">https://doi.org/10.1177/1535370220928275</a>
Issue Date	2020-06-01
Doc URL	<a href="http://hdl.handle.net/2115/79023">http://hdl.handle.net/2115/79023</a>
Rights	Masaya Hiraishi, Md Abdul Masum, Takashi Namba, Yuki Otani, Yaser HA Elewa, Osamu Ichii, Yasuhiro Kon, Histopathological changes in tear-secreting tissues and cornea in a mouse model of autoimmune disease, Experimental Biology and Medicine (Volume 245 Issue 12) pp. 999-1008. Copyright © 2020 the Society for Experimental Biology and Medicine (SEBM). DOI: 10.1177/1535370220928275
Type	article (author version)
Additional Information	There are other files related to this item in HUSCAP. Check the above URL.
File Information	Manuscript.pdf



[Instructions for use](#)

1   **Histopathological changes in tear-secreting tissues and cornea in a mouse model of**  
2   **autoimmune disease**

3

4   **Short title: Histopathology of tear-secreting tissues**

5

6   Masaya Hiraishi<sup>1\*</sup>, Md. Abdul Masum<sup>1,2\*</sup>, Takashi Namba<sup>1</sup>, Yuki Otani<sup>1</sup>, Yaser Hosny Ali  
7   Elewa<sup>1,3</sup>, Osamu Ichii<sup>1,4#</sup>, and Yasuhiro Kon<sup>1</sup>.

8   1.   Laboratory of Anatomy, Department of Basic Veterinary Sciences, Faculty of Veterinary  
9       Medicine, Hokkaido University, Sapporo, 060-0618, Japan

10   2.   Department of Anatomy, Histology and Physiology, Faculty of Animal Science and  
11       Veterinary Medicine, Sher-e-Bangla Agricultural University, Dhaka, 1207, Bangladesh

12   3.   Department of Histology, Faculty of Veterinary Medicine, Zagazig University, Zagazig,  
13       44519, Egypt

14   4.   Laboratory of Agrobiomedical Regenerative Medicine, Faculty of Agriculture, Hokkaido  
15       University, Sapporo, 060-8589, Japan

16

17   \* Hiraishi M and Masum MA equally contributed to this paper

18   # Corresponding author:

19   Osamu Ichii, DVM, PhD

20   Laboratory of Anatomy, Department of Basic Veterinary Sciences, Faculty of Veterinary  
21       Medicine, Hokkaido University, Kita 18, Nishi 9, Kita-ku, Sapporo 060-0818, Japan

22   Email: ichi-o@vetmed.hokudai.ac.jp

23   Tel: +81-11-706-5189, Fax: +81-11-706-5189

24     **Abstract**

25     The tear film covers the cornea, and its abnormalities (including immunological) induce dry  
26     eye. Using autoimmune disease model mice, BXSB/MpJ-Yaa (BXSB-Yaa), histopathological  
27     changes in the eye and tear-secreting tissues were examined using histopathology,  
28     immunohistochemistry, and electron microscopy at 8, 20, and 28 weeks for early, middle, and  
29     late disease stages. Early and middle stage BXSB-Yaa showed increased serum autoantibody  
30     and spleen to body weight (S/B), respectively, and higher tear volume than controls, BXSB/MpJ  
31     (BXSB), at early stages, which decreased with ageing and negatively correlated with  
32     autoimmune disease indices. Late stage BXSB-Yaa showed smaller Meibomian gland acini, less  
33     intraorbital lacrimal gland, and smaller Harderian gland acinar cells than BXSB; the latter two  
34     indices decreased with ageing and negatively correlated with S/B. Cell infiltration occurred in  
35     the middle stage BXSB-Yaa extraorbital lacrimal gland, and acinar cells were smaller than  
36     BXSB. The conjunctiva goblet cells decreased from early to middle stages in both strains, but in  
37     BXSB-Yaa, they increased at late stages with a partial lack of microvilli on the cornea and were  
38     inversely altered with anterior epithelium thickness through ageing, suggesting that they  
39     compensated for anterior epithelium damage. In conclusion, the tear film was unstable due to an  
40     autoimmune disease condition in BXSB-Yaa.

41

42     **Keywords**

43     Tear film, Cornea, Autoimmune disease, BXSB/MpJ-Yaa mice

44     **Impact statement**

45     Cornea, an outermost layer of mammalian eye, is protected by tear film and abnormalities of  
46     tear film causes dry eye. Dry eye injures the cornea which results lower vision in patients.  
47     Several factors cause dry eye, including altered systemic conditions, environment, and  
48     immunological abnormality of the patient in autoimmune disease like Sjögren's syndrome (SS).  
49     However, the detailed pathology of autoimmune abnormality-mediated dry eye is unclear. Here  
50     we demonstrated that systemic autoimmune abnormality in BXSB-Yaa mice was associated  
51     with histological changes in the exocrine glands and cornea of the eyes. We also showed that  
52     BXSB-Yaa mice developed mild or early stage dry eye-like disease and explain the existence of  
53     a compensatory mechanism associated with the dysfunction of these tissues. Thus, BXSB-Yaa  
54     could be a model for SS-like disease-associated dry eye and these data would contribute to the  
55     understanding of the pathogenesis of autoimmune-related dry eye disease.

56

57     **Introduction**

58       For mammalian eyeballs, the outermost cornea is covered and protected by the tear film  
59       composed of mucin, water, and lipid layers from its inner side. Secretions from conjunctival  
60       goblet cells, lacrimal glands (LGs), and the Meibomian gland (MG) contribute to the formation  
61       of the tear film.<sup>1-3</sup> The deep gland of the third eyelid, known as the Harderian gland (HG), also  
62       contributes to the formation of the lipid layer.<sup>4</sup> Dysfunction or injuries in these tear film-forming  
63       cells cause several eye diseases. Loss of conjunctival goblet cells and dysfunction of the LG as  
64       well as the MG causes the disruption of the water layer, since the latter is crucial to prevent the  
65       evaporation of water.<sup>5-7</sup> In general, eye diseases due to tear film abnormalities are diagnosed as  
66       “dry eye” in humans and animals.

67       Dry eye injures the cornea in humans and companion animals; model animals of dry eye  
68       have been reported.<sup>8-10</sup> This disease reduces the quality of life in patients because it causes  
69       fatigue or pain of the eyes and eventually leads to low vision. Dry eye is known as a chronic  
70       disease associated with keratoconjunctivitis. Several factors cause dry eye, including altered  
71       systemic conditions, environment, ophthalmic operation, and an immune abnormality of the  
72       patient.<sup>11-14</sup> Sjögren’s syndrome (SS), a representative autoimmune disease targeting exocrine  
73       glands, causes dry eye in humans.<sup>15</sup> Between 0.04 and 3.1 million adults suffer from SS in the  
74       United States.<sup>16</sup> While SS is not fatal, approximately 5% of patients with long-term SS develop  
75       malignant lymphoma.<sup>17-19</sup> Companion dogs that show dry eye associated with an autoimmune  
76       disorder have SS-like disease.<sup>20,21</sup> For dry eye in SS, autoimmune abnormality-associated  
77       inflammation in the LGs, MG dysfunction, and goblet cell loss are reported in human patients  
78       and model animals.<sup>22-27</sup> SS model mice have inflammation in the HG.<sup>28</sup> In Japan, SS is  
79       diagnosed in patients exhibiting more than two of the following characteristics: lymphocyte  
80       infiltration in labial salivary glands or LGs; hyposecretion of saliva; hyposecretion of tear fluid  
81       or an injured cornea; and anti-Ro/SS-A and anti-La/SS-B antibodies in the serum.

82 To elucidate the pathology of SS, the use of an animal model is crucial. The BXSB/MpJ-  
83 *Yaa* (BXSB-Yaa) mouse, carrying the Y-linked autoimmune accelerator (*Yaa*) mutation on the Y  
84 chromosome, is a representative autoimmune disease model and develops severe symptoms,  
85 including abnormal proliferation of B-cells, autoantibody production, splenomegaly, and  
86 glomerulonephritis.<sup>29-31</sup> BXSB-Yaa manifests SS-like symptoms, such as B-cell predominant  
87 lymphocytic infiltrations and the destruction of acini in extraorbital lacrimal glands (ELGs).<sup>22</sup> In  
88 that study, there was no significant difference in the quantity of tear production between BXSB-  
89 *Yaa* and healthy C57BL/6 mice, suggesting that BXSB-Yaa could be a model for mild or early  
90 stage dry eye. However, the detailed pathology of autoimmune abnormality-mediated dry eye is  
91 unclear since no study has elucidated the histopathological changes in tear-secreting tissues  
92 using SS model mice.

93 We investigated the histopathology of tear-secreting tissues and cornea in BXSB-Yaa mice,  
94 evaluating autoimmune disease development and tear production by comparing them to the  
95 healthy control strain BXSB/MpJ (BXSB). We found that BXSB-Yaa mice developed mild or  
96 early stage dry eye-like disease and discuss the existence of a compensatory mechanism  
97 associated with the dysfunction of these tissues in this model. These data contribute to the  
98 understanding of the pathogenesis of autoimmune-related dry eye disease.

99     **Materials and Methods**

100    *Animals*

101       Male BXSB and BXSB-Yaa mice aged 8, 20, 24, and 28 weeks were purchased from Japan  
102       SLC, Inc. (Hamamatsu, Japan) and maintained under specific pathogen-free conditions. Animal  
103       experimentation was approved by the Institutional Animal Care and Use Committee of the  
104       Faculty of Veterinary Medicine, Hokkaido University (approval No. 16-0124). All experimental  
105       animals were handled in accordance with the Guide for the Care and Use of Laboratory  
106       Animals, Faculty of Veterinary Medicine, Hokkaido University (approved by the Association  
107       for Assessment and Accreditation of Laboratory Animal Care International).

108

109    *Sample collection*

110       Under deep anaesthesia, using a mixture of medetomidine (0.3 mg/kg), midazolam (4  
111       mg/kg), and butorphanol (5 mg/kg), tears were collected using Schirmer test paper (Schirmer  
112       Tear Production Measuring Strips; Showa Yakuhin, Tokyo, Japan), which was sliced at  
113       approximately 1 mm width and inserted into the lower conjunctival sac for 4 min. Then, blood  
114       was collected from the femoral arteries, and all mice were euthanized by cervical dislocation.  
115       The heads, eyeballs, periocular tissues, and spleens were immediately collected and used for  
116       further analysis.

117

118    *Tear volume measurement*

119       Tear volume was measured according to a previous report.<sup>22</sup> Briefly, using a digital image,  
120       the tear-wetted area of Schirmer test paper was measured using ImageJ (NIH,  
121       <http://rsbweb.nih.gov/ij/>) and estimated as the tear volume.

122

123    *Serological analysis*

124       Serum levels of anti-double-stranded DNA (dsDNA) antibody were measured to evaluate

125 systemic autoimmune conditions and disease development using the LBIS Anti-dsDNA-Mouse  
126 ELISA Kit (FUJIFILM Wako Pure Chemical Corporation; Osaka, Japan) according to the  
127 manufacturer's instructions.

128

129 ***Histopathological analysis***

130 The eyeballs with conjunctiva, MG, and HG were fixed with 4% paraformaldehyde (PFA)  
131 at 4 °C overnight. The tissues were dehydrated using alcohol and embedded in paraffin, cut into  
132 3-μm-thick sections, and stained with haematoxylin-eosin (HE). Sections of the eyeball with  
133 conjunctiva were stained with periodic acid-Schiff (PAS). The skulls including intraorbital  
134 lacrimal gland (ILG), and ELG were immersed in acetone overnight to eliminate lipids after  
135 fixation with 4% PFA. Then, they were immersed in 10% formic acid for 12 h to decalcify.  
136 Paraffin sections (3-μm-thick) were prepared and stained with HE or PAS.

137

138 ***Histoplanimetry***

139 HE-stained sections were converted to virtual slides using Nano Zoomer 2.0 RS  
140 (Hamamatsu Photonics Co., Ltd.; Hamamatsu, Japan), and then each measurement was  
141 performed using NDP.view2 software (Hamamatsu Photonics Co., Ltd.). The number of MG  
142 acini in the upper tarsal plates in the defined area ( $445 \times 352 \mu\text{m}$ ) was counted for two areas and  
143 expressed as MG acinus density. For the HG, ELG, and ILG, the area of the acinus (1) and its  
144 ductal lumen (2) was measured by drawing a line on NDP.view2 (Hamamatsu Photonics Co.,  
145 Ltd.); the size of one acinus was obtained by subtracting (2) from (1). This measurement was  
146 performed randomly for 50 acini in the HG and ELG, and 30 acini in the ILG, for each sample.  
147 For the palpebral conjunctiva, goblet cell density in the conjunctiva epithelium was calculated  
148 from the number of goblet cells within the length of two non-overlapping areas from the upper  
149 and lower eyelids (more than  $500 \mu\text{m}$ ). We also measured the thickness of the anterior  
150 epithelium of the cornea at five points around the central part of the cornea.

151     ***Immunohistochemistry***

152       Paraffin sections were deparaffinized and antigen retrieval was performed. The sections  
153       were soaked in methanol containing 0.3% H<sub>2</sub>O<sub>2</sub> for 20 min at room temperature to remove  
154       internal peroxidase. After washing three times in phosphate buffered saline (PBS), sections were  
155       incubated with blocking serum for 1 h at room temperature and primary antibodies overnight at  
156       4 °C. Prior to, and after sections were incubated with secondary antibodies for 30 min at room  
157       temperature, they were washed three times in PBS. The sections were incubated with  
158       streptavidin-conjugated horseradish peroxidase (SABPO(R) kit; Nichirei, Tokyo, Japan) for 30  
159       min and washed three times in PBS. For visualisation of the positive reactions, the sections were  
160       incubated with 10 mg 3, 3'-diaminobenzidine tetrahydrochloride in 50 mL 0.05 M Tris-HCl  
161       buffer-H<sub>2</sub>O<sub>2</sub> solution. Finally, sections were stained with haematoxylin. Antibodies, antigen  
162       retrieval, and blocking details are listed in Supplementary Table 1.

163

164     ***Scanning electron microscopy (SEM)***

165       Whole eyeball samples from BXSB and BXSB-Yaa at 28 weeks of age were pre-fixed with  
166       2.5% glutaraldehyde in 0.1 M phosphate buffer (PB) for 4 h at 4 °C. Then, the samples were  
167       washed five times with 0.1 M PB for 10 min each. The samples were post-fixed with 1% OsO<sub>4</sub>  
168       for 1 h, immersed in 1% tannic acid solution (TAS) for 1.5 h as a conductive treatment, and  
169       washed six times with 0.1 M PB for 10 min each at 4 °C. Then, the samples were post-fixed in  
170       1% OsO<sub>4</sub> for 1 h again and washed again, as above. Subsequently, the samples were immersed  
171       in 0.5% TAS for 10 min and then 1.0% TAS for 1 h at 4 °C. After washing in 0.1 M PB, the  
172       specimens were dehydrated with graded ethanol, replaced with isoamyl acetate, and dried using  
173       a critical point drier (HCP-2, Hitachi; Tokyo, Japan). The dried specimens were mounted on  
174       aluminium stubs, treated by ion sputtering (E-1030, Hitachi), and observed using an SEM (SU  
175       8000, Hitachi; 10 kV).

176     ***Statistical analysis***

177       The results are expressed as the mean  $\pm$  standard error (SE). Analysis between two groups  
178      was conducted using the Mann-Whitney *U*-test. Multiple comparisons over three groups were  
179      conducted using Scheffé's method after the Kruskal-Wallis test. The correlation between two  
180      parameters was analysed using Spearman's correlation test. In all analyses,  $P < 0.05$  was  
181      regarded as significantly different.

182    **Results**

183    ***Autoimmune disease indices and tear volume***

184    BXSB-Yaa mice at 8, 20, and 28 weeks of age were investigated as models of early, moderate,  
185    and late stage autoimmune disease, respectively. BXSB-Yaa showed significantly higher ratios  
186    of spleen weight to body weight (S/B) than BXSB at 20 weeks; BXSB-Yaa at 28 weeks showed  
187    significantly higher S/B than BXSB-Yaa at 8 weeks (Figure 1A). The serum levels of anti-  
188    dsDNA antibody were significantly higher in BXSB-Yaa than in BXSB at all examined weeks  
189    without age-related significant differences (Figure 1B). Although BXSB showed no significant  
190    age-related changes, tear volume in BXSB-Yaa decreased with age and showed a significant  
191    difference between 8 and 20 or 28 weeks (Figure 1C), and a significantly higher value than  
192    BXSB at 8 weeks.

193

194    ***Histopathology of MG and HG, lipid layer composing exocrine glands***

195    As shown in Figure 2A, MGs are observed as a cluster of foamy sebaceous gland cells  
196    beneath the palpebral conjunctiva in the upper or lower tarsal plates. Melanin pigments were  
197    observed between the MG acini. No change in acinus morphology was observed among ages or  
198    strains, but the number of acini in BXSB-Yaa was lower than that in BXSB at all ages. The HG  
199    acini in the third eyelid were composed of clear glandular epithelial cells containing numerous  
200    minute lipids in their abundant cytoplasm (Figure 2B). Further, brown-coloured porphyrins were  
201    observed in some acinar lumens. No change was observed in porphyrin appearance among ages  
202    or strains; the size of acinus decreased from 20 weeks in BXSB-Yaa, but not in BXSB.  
203    Inflammatory cell infiltrations in MG and HG were not obvious in all ages of both strains.

204    MG acinar density and HG acinar size in BXSB-Yaa were lower than those in BXSB at 8  
205    and 20 weeks (Figure 2C and D); significant strain differences were detected at 28 weeks for  
206    both parameters. In BXSB-Yaa, HG values were significantly decreased from 8 weeks to 20 and

207 28 weeks (Figure 2D).

208

209 ***Histopathology of ELG and ILG, water layer composing exocrine glands***

210 Figure 3 shows the histopathological observation of LGs. For ELGs (Figure 3A), serous  
211 acini were composed of glandular epithelial cells with a clear and large cytoplasm in the apical  
212 portion and a basophilic one in the basal portion. The size of nuclei in acinar epithelial cells or  
213 acinar lumens differed among acini, but there was no consistent difference among ages or  
214 strains. Although the histological characteristics of ILG were similar to those of ELGs, the ILG  
215 acinus was smaller than that of ELG, and the ILG was separated into smaller lobules than the  
216 ELG (Figure 3B). No change was observed in ELGs and ILGs of BXSB of all ages, but smaller  
217 acini were found in BXSB-Yaa at 20 and 28 weeks than those at 8 weeks.

218 ELG and ILG acinar sizes in BXSB-Yaa were both lower than those in BXSB at 20 weeks,  
219 but the reduction in ELG acinar size was significant (Figure 3C and D). In BXSB, the ELG  
220 showed increased acinar sizes with age without statistical significance, but in BXSB-Yaa, ILG  
221 values significantly decreased from 8 weeks to 20 and 28 weeks (Figure 3D).

222 Since several mononuclear cells are observed between the acini of ELGs, particularly  
223 around the ducts, as shown in Figure 3A and previous reports,<sup>17</sup> cell infiltration was evaluated.  
224 In all samples, ELGs had cell infiltration at 8, 20, and 28 weeks in BXSB (0/4, 1/4, 2/4 animals,  
225 respectively) and BXSB-Yaa (0/4, 4/4, 4/4 animals, respectively). Using immunohistochemistry,  
226 these inflammatory cells comprised B220<sup>+</sup> B-cells, CD3<sup>+</sup> T-cells, and Iba1<sup>+</sup> macrophages (Figure  
227 4A-C). For ILG, cell infiltration was scarce, but one sample from BXSB-Yaa at 20 weeks (1/4  
228 animals) showed cell infiltration. These lesions comprised B220<sup>+</sup> B-cells, CD3<sup>+</sup> T-cells, and  
229 Iba1<sup>+</sup> macrophages, similar to ELG (Figure 4D).

230

231 ***Histopathology of goblet cells in the palpebral conjunctiva and mucin layer composing cells***

232 In all mice, the palpebral or forniceal conjunctiva was composed of stratified cuboidal to

233 columnar epithelium (Figure 5A). Several PAS-positive goblet cells were observed in the  
234 epithelium of the palpebral or forniceal conjunctiva. For the palpebral conjunctiva, there was no  
235 morphological difference between the upper and lower eyelids. In BXSB, the number of PAS<sup>+</sup>  
236 palpebral conjunctiva goblet cells decreased at 20 and 28 weeks compared to those at 8 weeks.  
237 Goblet cell numbers also decreased in BXSB-Yaa from 8 to 20 weeks but increased again at 28  
238 weeks. Figure 5B shows the goblet cell density in the palpebral conjunctiva. In BXSB-Yaa,  
239 PAS<sup>+</sup> conjunctiva goblet cells significantly decreased from 8 to 20 weeks but increased from 20  
240 to 28 weeks, without statistical significance. At 28 weeks, BXSB-Yaa showed significantly  
241 higher values than BXSB.

242

243 ***Histopathology of the cornea***

244 The cornea is composed of the anterior epithelium, the proper substance, the posterior  
245 limiting membrane (Descemet's membrane), and the posterior epithelium from the outside, as  
246 shown in Figure 6A. The anterior epithelium is stratified squamous epithelium with 5-7 cell  
247 layers, which is influenced by changes in the tear film,<sup>32</sup> and it thickened with ageing in BXSB,  
248 but not in BXSB-Yaa (Figure 6A). BXSB, but not BXSB-Yaa, had significantly increased  
249 thickness of the anterior corneal epithelium from 8 weeks to 20 weeks, but the epithelium in  
250 BXSB-Yaa was significantly thinner than that in BXSB at 28 weeks (Figure 6B).

251 SEM analysis of the ultrastructure of the corneal surface was performed in BXSB and  
252 BXSB-Yaa at 28 weeks (Figure 6C). Under low magnification, BXSB showed a smooth and flat  
253 surface while BXSB-Yaa showed a few dark areas. High magnification analysis revealed that  
254 the surface of the cornea was covered by numerous microvilli in BXSB, but the dark area,  
255 observed under low magnification, lacked intact microvilli in 75% of examined BXSB-Yaa  
256 (n=4).

257

258 ***Correlation among tear volume, autoimmune disease indices, and altered tear-secreting***

259 *tissue morphologies*

260 The correlations among tear volumes, the indices of autoimmune disease, and tear-  
261 secreting tissue morphologies are summarised in Table 1. For all mice, tear volume showed no  
262 correlations with any parameters, but S/B and anti-dsDNA antibody were significantly and  
263 negatively correlated with MG and HG histological parameters. S/B also correlated with ELG  
264 and ILGs, indicating the relationship between autoimmune disease development and  
265 histopathological alterations.

266 BXSB-Yaa tear volume was significantly and positively correlated with ILG histological  
267 parameters, and S/B significantly and negatively correlated with HG and ILG histological  
268 parameters, as well as tear volume, showing age-related decreases in this strain. This result  
269 correlates autoimmune disease progression with alteration of tear volume and morphological  
270 changes in these organs. Moreover, our correlation analysis revealed that corneal  
271 histopathological parameter was only significantly and negatively correlated with conjunctival  
272 goblet cells in all mice and BXSB-Yaa mice (Supplemental Table 1).

273 **DISCUSSION**

274 BXSB-Yaa showed increased serum levels of anti-dsDNA antibody and S/B from 8 to 20  
275 weeks, indicating the onset of autoimmune abnormality started from 8 weeks. Although the tear  
276 volume index decreased with age in BXSB-Yaa, these mice showed higher values than BXSB at  
277 8 weeks. The Schirmer test paper indicated basal as well as reflex secretion of tears due to the  
278 physical stimuli of paper insertion into the conjunctival sac.<sup>22</sup> Therefore, the altered tear volume  
279 in BXSB-Yaa suggested a change in basal and/or reflex secretion from tear-producing  
280 components. At 8 weeks, there was no significant difference in the tear film- or cornea-  
281 associated histoplanimetry between the two strains, but BXSB-Yaa showed a lower MG acinar  
282 density, an important component forming the tear film lipid layer. Tear volume increases to  
283 compensate for the decreased lipid layer in stearoyl coenzyme A desaturase-1 (SCD-1) deficient  
284 mice, which lack the enzyme related to lipid synthesis and suffer from MG dysfunction.<sup>33</sup> Tear  
285 volume and autoimmune indices were significantly and negatively correlated in BXSB-Yaa.  
286 Thus, we hypothesised that tear volume increased to compensate for the decreased lipid layer  
287 from MG dysfunction in young BXSB-Yaa and decreased with the progression of autoimmune  
288 disease and the altered function of tear film-producing organs.

289 In aged BXSB-Yaa (middle and late stage), altered acinar morphology was observed in  
290 ELG and ILG, the water layer-producing components. Cell infiltration in these LGs was  
291 observed in BXSB-Yaa but not in BXSB. The destruction of LGs and salivary glands in SS  
292 model mice is mediated by cytokines, such as interleukins or interferons, secreted from  
293 infiltrating lymphocytes.<sup>34</sup> In BXSB-Yaa, the histological changes in ILG, but not ELG,  
294 significantly correlated with tear volume and S/B, suggesting the close relationship with altered  
295 ILG morphology and autoimmune disease or tear production in mice, although ELG showed  
296 more cell infiltration than ILG. Only the LGs, but not other organs, showed obvious  
297 inflammatory features, even though HG and MG morphology was altered in ageing BXSB-Yaa.

298 Thus, lipid- and water layer-producing organs showed different pathological processes; further  
299 study is needed to elucidate the mechanism. Moreover, clarification of cellular cluster around  
300 the duct as tertiary lymphoid cluster might add value to identify the pathogenesis of  
301 histomorphological changes of LG.

302 Age-related changes in HG, ELG, ILG and conjunctiva goblet cell histopathological  
303 indices in BXSB-Yaa at 20 weeks indicated their altered morpho-function, assuming they were  
304 associated with tear film stability. While the anterior corneal epithelium thickened from 8 to 20  
305 weeks in both strains, it was thinner in BXSB-Yaa than in BXSB at 28 weeks. Consistent with  
306 our results, the anterior corneal epithelium thickens with ageing in healthy mice,<sup>35</sup> and dry eye  
307 model mice have thinner corneal epithelium due to cell injuries than healthy controls.<sup>10</sup> Previous  
308 study showed that tear film instability potential damaged to the ocular surface.<sup>32</sup> Our SEM data  
309 also revealed that several areas on the corneal surface lacked microvilli in aged-BXSB-Yaa,  
310 which might reflect corneal injury at 28 weeks due to the unstable tear film.

311  
312 The density of conjunctiva goblet cells and mucin layer-associated cells decreased from 20  
313 weeks in BXSB. Conjunctival goblet cell density decreases in healthy mice with ageing.<sup>36</sup> Cell  
314 density in BXSB-Yaa decreased from 8 to 20 weeks but recovered at 28 weeks. At 28 weeks, the  
315 BXSB-Yaa group developed prominent autoimmune disease abnormalities that significantly  
316 altered tear film-producing organs, including MG, HG, ILG, and the cornea. Moreover,  
317 inflammatory cytokines associated with SS contributes to dry eye by inducing apoptosis and  
318 increasing mucin secretion and conjunctival goblet cell proliferation.<sup>37</sup> Therefore, we  
319 hypothesised that increased goblet cells in BXSB-Yaa at 28 weeks compensated for their altered  
320 morpho-function. In fact, SCD-1 deficient mice, which exhibit MG dysfunction, show a  
321 compensatory increase in mucin levels in their tears.<sup>33</sup> Our correlation analysis revealed that  
322 conjunctival goblet cells and corneal histopathological parameters showed significant and  
323 negative correlations in all mice ( $\rho=-0.685, P < 0.01$ ) and BXSB-Yaa ( $\rho=-0.748, P < 0.01$ ),

324 supporting this compensation theory.

325 Here, BXSB-Yaa satisfied at least two of the Japanese SS diagnostic criteria: lymphocytic  
326 infiltration in LGs and corneal injury. Therefore, BXSB-Yaa could be a model for SS-like  
327 disease, even if lacrimal hyposecretion did not develop. SS-like disease in model mice  
328 progresses according to three phases.<sup>38</sup> Phase 1 shows increased apoptosis of acinar cells and  
329 abnormal protein or gene expression. Phase 2 shows inflammatory cell infiltration into the  
330 exocrine gland and autoantibody production. Phase 3 shows loss of secretory function  
331 progression, as found in dry eye. Based on this study, and another,<sup>22</sup> BXSB-Yaa developed  
332 phase 2 SS. This autoimmune disease-prone strain would likely develop dry eye because tear  
333 volume significantly decreases with ageing in these mice.

334 In conclusion, we demonstrated that systemic autoimmune abnormality in BXSB-Yaa was  
335 associated with histological changes in the exocrine glands and cornea of the eyes. Thus,  
336 BXSB-Yaa could be a model for mild stage SS-like disease-associated dry eye. Further studies  
337 focusing on the cause of morphological or detailed functional changes in tear-secreting glands  
338 would elucidate the pathology of SS-associated symptoms in human and veterinary medicine.

339    **Authors' contributions**

340    M.H., M.A. M., T. N., Y. O., Y. H. A. E, O.I., and Y.K. designed and performed experiments.

341    M.H. and M.A. M. analysed the data. All authors were involved in writing the paper and

342    approved the final manuscript.

343    **Acknowledgement**

344    This research was awarded the Encouragement Award (undergraduate section) at the 162<sup>nd</sup>

345    Japanese Association of Veterinary Anatomists in Tsukuba, Japan (September 2019).

346

347    **Declaration of conflicting interests**

348    The authors declared no potential of interest with respect to the research, authorship, and/or

349    publication of this article.

350

351    **Funding**

352    This research received no specific grant from any funding agency in the public, commercial, or

353    not-for-profit sectors.

354 **FIGURE LEGENDS**

355 **Figure 1. Indices for autoimmune abnormality and tear volume in mice.**

356 (A) The ratio of spleen weight to body weight.

357 (B) The serum levels of anti-double stranded DNA (dsDNA) antibody.

358 (C) Tear volume

359 BXSB: BXSB/MpJ. BXSB-Yaa: BXSB/MpJ-Yaa. Each bar represents the mean  $\pm$  SE (n = 4).

360 \*: Significant strain difference at the same age, Mann-Whitney U-test. †: Significant difference  
361 from the other groups, Kruskal-Wallis test followed by Scheffe's method.

362

363 **Figure 2. Histopathology of lipid layer-composing exocrine glands in mice.**

364 (A) Meibomian glands (MGs) in the upper tarsal plate. Sebaceous gland cells form clusters  
365 beneath the conjunctival epithelium (CE). Melanin pigments indicated by arrowheads are  
366 observed between and around acinar cells. CS: conjunctival sac. Cor: Cornea. HE staining.  
367 Bars = 100  $\mu$ m.

368 (B) Harderian glands (HGs) in the third eyelid. Acini of HGs are composed of clear glandular  
369 epithelial cells containing numerous minute lipids in their abundant cytoplasm. Some acini  
370 include porphyrins in their lumens. Arrowheads point to porphyrin. Smaller acinar  
371 epithelial cells are observed in BXSB-Yaa at 20 and 28 weeks. HE staining. Bars = 100  
372  $\mu$ m.

373 (C) MG acinus density.

374 (D) The size of one acinus in HGs.

375 BXSB: BXSB/MpJ. BXSB-Yaa: BXSB/MpJ-Yaa Each bar represents the mean  $\pm$  SE (n = 4).

376 \*: Significant strain difference at the same age, Mann-Whitney U-test. †: Significant difference  
377 from the other groups, Kruskal-Wallis test followed by Scheffe's method.

378

379 **Figure 3. Histopathology of water layer-composing exocrine glands in mice.**

380 (A) Extraorbital lacrimal glands (ELGs). Each acinus is composed of serous cells and a small  
381 lumen. Mononuclear cells (arrowheads) are observed around the ducts (arrows). Smaller  
382 acini are observed in BXSB-Yaa at 20 and 28 weeks. HE staining. Bars = 100  $\mu$ m.  
383 (B) Intraorbital lacrimal glands (ILGs). Histological characteristics are similar to those of ELG.  
384 These glands are separated into smaller lobules. Smaller acini are observed in BXSB-Yaa at  
385 20 and 28 weeks. HE staining. Bars = 100  $\mu$ m.  
386 (C) Size of one acinus in ELGs.  
387 (D) Size of one acinus in ILGs.  
388 BXSB: BXSB/MpJ. BXSB-Yaa: BXSB/MpJ-Yaa Each bar represents the mean  $\pm$  SE (n = 4). \*  
389 \*: Significant strain difference at the same age, Mann-Whitney U-test. †: Significant difference  
390 from the other groups, Kruskal-Wallis test followed by Scheffe's method.  
391

392 **Figure 4. Inflammatory cell infiltration in lacrimal glands.**

393 (A-C) Immunohistochemistry for B220 (panel A), CD3 (panel B), and Iba1 (panel C) in  
394 extraorbital lacrimal glands. Positive cells localise around the ducts (arrowheads). Bars =  
395 100  $\mu$ m.  
396 (D) Immunohistochemistry for B220, CD3, and Iba1 in intraorbital lacrimal glands in BXSB-  
397 Yaa at 20 weeks of age. Bars = 100  $\mu$ m.  
398

399 **Figure 5. Histopathology of mucin layer-producing tissues in mice.**

400 (A) Palpebral conjunctiva in the upper or lower eyelids. PAS<sup>+</sup> goblet cells, indicated by  
401 arrowheads, are observed in the epithelium of the palpebral conjunctiva. The number of  
402 goblet cells decreased in BXSB with age, but not in BXSB-Yaa. PAS staining. Bars = 100  
403  $\mu$ m. CS: Conjunctival sac.  
404 (B) Goblet cell density in the conjunctival epithelium.  
405 BXSB: BXSB/MpJ. BXSB-Yaa: BXSB/MpJ-Yaa Each bar represents the mean  $\pm$  SE (n = 4). \*

406 \*: Significant strain difference at the same age, Mann-Whitney *U*-test. †: Significant difference  
407 from the other groups, Kruskal-Wallis test followed by Scheffe's method.

408

409

410 **Figure 6. Histopathology of cornea in mice.**

411 (A) Cornea histology. The cornea is composed of four layers: the anterior epithelium (AE), the  
412 proper substance (PS), Descemet's membrane (DM), and the posterior epithelium (PE).  
413 The anterior epithelia of the cornea thickened with age in BXSB, but not in BXSB-Yaa. HE  
414 staining. Bars (black) = 100  $\mu$ m. Bars (inset) = 20  $\mu$ m.

415 (B) Thickness of corneal AE.

416 (C) Scanning electron microscopy images of the anterior surface of the cornea. Numerous  
417 microvilli cover the surface of the cornea in BXSB, and they disappear in some areas in  
418 BXSB-Yaa at 28 weeks of age. The area without microvilli is surrounded by a dotted line.  
419 Bars = 5  $\mu$ m

420 BXSB: BXSB/MpJ. BXSB-Yaa: BXSB/MpJ-Yaa Each bar represents the mean  $\pm$  SE (n = 4). \*  
421 \*: Significant strain difference at the same age, Mann-Whitney *U*-test. †: Significant difference  
422 from the other groups, Kruskal-Wallis test followed by Scheffe's method.

423

424

425

426

427    **REFERENCES**

- 428    1. Walcott B. The lacrimal gland and its veil of tears. *News Physiol Sci* 1998; **13**: 97-103.
- 429    2. Shinomiya K, Ueta M and Kinoshita S. A new dry eye mouse model produced by exorbital  
430        and intraorbital lacrimal gland excision. *Sci Rep* 2018; **8**: 1483.
- 431    3. Foulks GN and Bron AJ. Meibomian gland dysfunction: A clinical scheme for description,  
432        diagnosis, classification, and grading. *Ocul Surf* 2003; **1**: 107–126.
- 433    4. Payne AP. The harderian gland: a tercentennial review. *J Anat* 1994; **185**: 1–49.
- 434    5. Barbosa FL, Xiao Y, Bian F, Coursey TG, Ko BY, Clevers H, de Paiva CS and Pflugfelder  
435        SC. Goblet cells contribute to ocular surface immune tolerance—implications for dry eye  
436        disease. *Int J Mol Sci* 2017; **18**: pii: E978.
- 437    6. Ralph RA. Conjunctival goblet cell density in normal subjects and in dry eye syndromes.  
438        *Invest Ophthalmol* 1975; **14**: 299–302.
- 439    7. Mishima S and Maurice DM. The oily layer of the tear film and evaporation from the  
440        corneal surface. *Exp Eye Res* 1961; **1**: 39–45.
- 441    8. Cui X, Hong J, Wang F, Deng SX, Yang Y, Zhu X, Wu D, Zhao Y and Xu J. Assessment  
442        of corneal epithelial thickness in dry eye patients. *Optom Vis Sci* 2014; **91**: 1446–1454.
- 443    9. Dodi P. Immune-mediated keratoconjunctivitis sicca in dogs: current perspectives on  
444        management. *Vet Med (Auckl)* 2015; **6**: 341-347.
- 445    10. Marques DL, Alves M, Modulo CM, da Silva LECM, Reinach P and Rocha EM. Lacrimal  
446        osmolaritu and ocular surface in experimental model of dry eye caused by toxicity. *Rev  
447        Bras Oftalmol* 2015; **74**: 68–72.
- 448    11. Alves M, Novaes P, Morraye MdeA, Reinach PS and Rocha EM. Is dry eye an  
449        environmental disease? *Arq Bras Oftalmol* 2014; **77**: 193–200.
- 450    12. Stevenson W, Chauhan SK and Dana R. Dry eye disease: and immune-mediated ocular  
451        surface disorder. *Arch Ophthalmol* 2012; **130**: 90-100.
- 452    13. Toda I. Dry eye after lasik. *Invest Ophthalmol Vis Sci* 2018; **59**: 109–115.

- 453 14. Wilkinson BR. Dry eye syndrome. *Ophthalmology* 1999; **106**: 1044.
- 454 15. Sjogren H. Keratoconjunctivitis sicca and chronic polyarthritis. *Acta Med Scand* 1948; **130**:
- 455 484-488.
- 456 16. Helmick CG, Felson DT, Lawrence RC, Gabriel S, Hirsch R, Kwoh CK, Liang MH,
- 457 Kremers HM, Mayes MD, Merkel PA, Pillemer SR, Reveille JD and Stone JH. Estimates
- 458 of the prevalence of arthritis and other rheumatic conditions in the United States. *Arthritis*
- 459 *Rheum* 2008; **58**: 15-25.
- 460 17. Ambrosetti A, Zanotti R, Pattaro C, Lenzi L, Chilosi M, Caramaschi P, Arcaini L, Pasini F,
- 461 Biasi D, Orlandi E, D'Adda M, Lucioni M and Pizzolo G. Most cases of primary salivary
- 462 mucosa-associated lymphoid tissue lymphoma are associated either with Sjögren
- 463 syndrome or hepatitis C virus infection. *Br J Haematol* 2004; **126**: 43-49.
- 464 18. de Vita S, Boiocchi M, Sorrentino D, Carbone A, Avellini C, Dolcetti R, Marzotto A,
- 465 Gloghini A, Bartoli E, Beltrami CA and Ferraccioli G. Characterization of
- 466 prelymphomatous stages of B cell lymphoproliferation in Sjögren's syndrome. *Arthritis*
- 467 *Rheum* 1997; **40**: 318-331.
- 468 19. Voulgarelis M and Moutsopoulos HM. Lymphoproliferation in autoimmunity and
- 469 Sjögren's syndrome. *Cur Rheum Rep* 2003; **5**: 317-32.
- 470 20. Nabeta R, Kambe N, Nakagawa Y, Chiba S, Xiantao H, Feruya T, Kishimoto M and
- 471 Uchide T. Sjögren's-like syndrome in a dog. *J Vet Med Sci* 2019; **81**: 886-889.
- 472 21. Quimby FW, Schwartz RS, Poskitt T and Lewis RM. A disorder of dogs resembling
- 473 Sjögren's syndrome. *Clin Immunol Immunopathol* 1979; **12**: 471-476.
- 474 22. Kosenda K, Ichii O, Otsuka S, Hashimoto Y and Kon Y. BXSB/MpJ-Yaa mice develop
- 475 autoimmune dacryoadenitis with the appearance of inflammatory cell marker messenger
- 476 RNAs in the lacrimal fluid. *Clin Exp Ophthalmol* 2013; **41**: 788-97.
- 477 23. Payne AP. The harderian gland: a tercentennial review. *J Anat* 1994; **185**: 1-49.
- 478 24. Hoffman RW, Alspaugh MA, Waggle KS, Durham JB and Walker SE. Sjögren's

- 479         Syndrome in MRL/l and MRL/n mice. *Arthritis Rheum* 1984; **27**: 157-65.
- 480     25. Sullivan DA, Dana R, Sullivan RM, Krenzer KL, Sahin A, Arica B, Liu Y, Kam WR,
- 481           Papas AS and Cermak JM. Meibomian gland dysfunction in primary and secondary
- 482           Sjögren Syndrome. *Ophthalmic Res* 2018; **59**: 193–205.
- 483     26. Wang C, Zaheer M, Bian F, Quach D, Swennes AG, Britton RA, Pflugfelder SC and de
- 484           Paiva CS. Sjögren-like lacrimal keratoconjunctivitis in germ-free mice. *Int J Mol Sci* 2018;
- 485           **19**: 565.
- 486     27. Williamson J, Gibson AA, Wilson TH, Forrester JV, Whaley KB and Dick WC. Histology
- 487           of the lacrimal gland in keratoconjunctivitis sicca. *Br J of Ophthalmol* 1973; **57**: 852–858.
- 488     28. Jabs DA, Alexander EL and Green WR. Ocular inflammation in autoimmune MRL/Mp
- 489           mice. *Invest Ophthalmol Vis Sci* 1985; **26**: 1223–1229.
- 490     29. Haywood ME, Rogers NJ, Rose SJ, Boyle J, McDermott A, Rankin JM, Thiruudaian V,
- 491           Lewis MR, Fossati-Jimack L, Izui S, Walport MJ and Morley BJ. Dissection of BXSB
- 492           lupus phenotype using mice congenic for chromosome 1 demonstrates that separate
- 493           intervals direct different aspects of disease. *J Immunol* 2004; **173**: 4277–4285.
- 494     30. Kimura J, Ichii O, Otsuka S, Sasaki H, Hashimoto Y and Kon Y. Close relations between
- 495           podocyte injuries and membranous proliferative glomerulonephritis in autoimmune murine
- 496           models. *Am J Nephrol* 2013; **38**: 27–38.
- 497     31. Pisitkun P, Deane JA, Difilippantonio MJ, Tarasenko T, Satterthwaite AB and Balland S.
- 498           Autoreactive B cell responses to RNA-related antigens due to TLR7 gene duplication.
- 499           *Science* 2006; **312**: 1669–1672.
- 500     32. Lam H, Bleiden L, de Paiva CS, Farley W, Stern ME and Pflugfelder SC. Tear cytokine
- 501           profiles in dysfunctional tear syndrome. *Am J Ophthalmol* 2009; **147**: 198-205.
- 502     33. Inaba T, Tanaka Y, Tamaki S, Ito T, Ntambi JM and Tsubota K. Compensatory increases
- 503           in tear volume and mucin levels associated with meibomian gland dysfunction caused by
- 504           stearoyl-CoA desaturase-1 deficiency. *Sci Rep* 2018; **8**: 3358.

- 505 34. Hayashi T. Dysfunction of lacrimal and salivary glands in Sjögren's syndrome:  
506 Nonimmunologic injury in preinflammatory phase and mouse model. *J Biomed Biotechnol*  
507 2011; **2011**: 407431.
- 508 35. Inomata T, Mashaghi A, Hong J, Nakao T and Dana R. Scaling and maintenance of corneal  
509 thickness during aging. *PLoS One* 2017; **12**: e0185694.
- 510 36. Volpe EA, Henriksson JT, Wang C, Barbosa FL, Zaheer M, Zhang X, Pflugfelder SC and  
511 de Paiva CS. Interferon-gamma deficiency protects against aging-related goblet cell loss.  
512 *Oncotarget* 2016; **7**: 64605–64614.
- 513 37. Contreras-Ruiz L, Ghosh-Mitra A, Shatos MA, Dartt DA and Masli S. Modulation of  
514 conjunctival goblet cell function by inflammation cytokines. *Mediators Inflamm* 2013; **2013**:  
515 636812.
- 516 38. Lee BH, Tudares MA and Nguyen CQ. Sjögren's syndrome: An old tale with a new twist.  
517 *Arch Immunol Ther Exp* 2009; **57**: 57–66.

1 Table 1. Correlations among tear volume, autoimmune disease indices, and altered tear-secreting tissue morphologies.

			Tear volume	Lipid		Water		Mucin	Cornea
				MG	HG	ELG	ILG	Conjunctiva	
<b>All</b>	Tear volume	$\rho$	1.000	-0.219	0.161	-0.009	0.323	-0.050	0.015
		P	-	0.304	0.453	0.968	0.124	0.816	0.944
	S/B	$\rho$	-0.184	-0.481*	-0.591**	-0.418*	-0.475*	0.176	-0.157
		P	0.391	0.017	0.002	0.042	0.019	0.412	0.465
	Anti-dsDNA antibody	$\rho$	-0.085	-0.619**	-0.436*	-0.388	-0.286	-0.109	-0.117
		P	0.694	0.001	0.033	0.061	0.175	0.612	0.588
<b>BXSB-Yaa</b>	Tear volume	$\rho$	1.000	-0.360	0.455	0.161	0.587*	-0.098	-0.077
		P	-	0.25	0.138	0.618	0.045	0.762	0.812
	S/B	$\rho$	-0.930**	0.322	-0.664*	-0.315	-0.608*	0.119	0.182
		P	0	0.308	0.018	0.319	0.036	0.713	0.572
	Anti-dsDNA antibody	$\rho$	-0.657*	0.265	-0.126	-0.224	-0.545	-0.420	0.420
		P	0.02	0.405	0.697	0.484	0.067	0.175	0.175

3 Spearman's rank correlation coefficients \*:  $P < 0.05$ , \*\*:  $P < 0.01$ .

4 All mice (n = 24), BXSB-Yaa: BXSB/MpJ-Yaa (n = 12)

5 S/B: The ratio of spleen weight to body weight, Tear: Tear volume, MG: MG acinus density, HG: The size of one acinus in the Harderian gland,

6 ELG: The size of one acinus in the extraorbital lacrimal gland, ILG: The size of one acinus in the intraorbital lacrimal gland, Conjunctiva: The goblet

7 cell density in the conjunctiva epithelium; Cornea: the thickness of the corneal anterior epithelium; -: not determined.

8

Figure 1

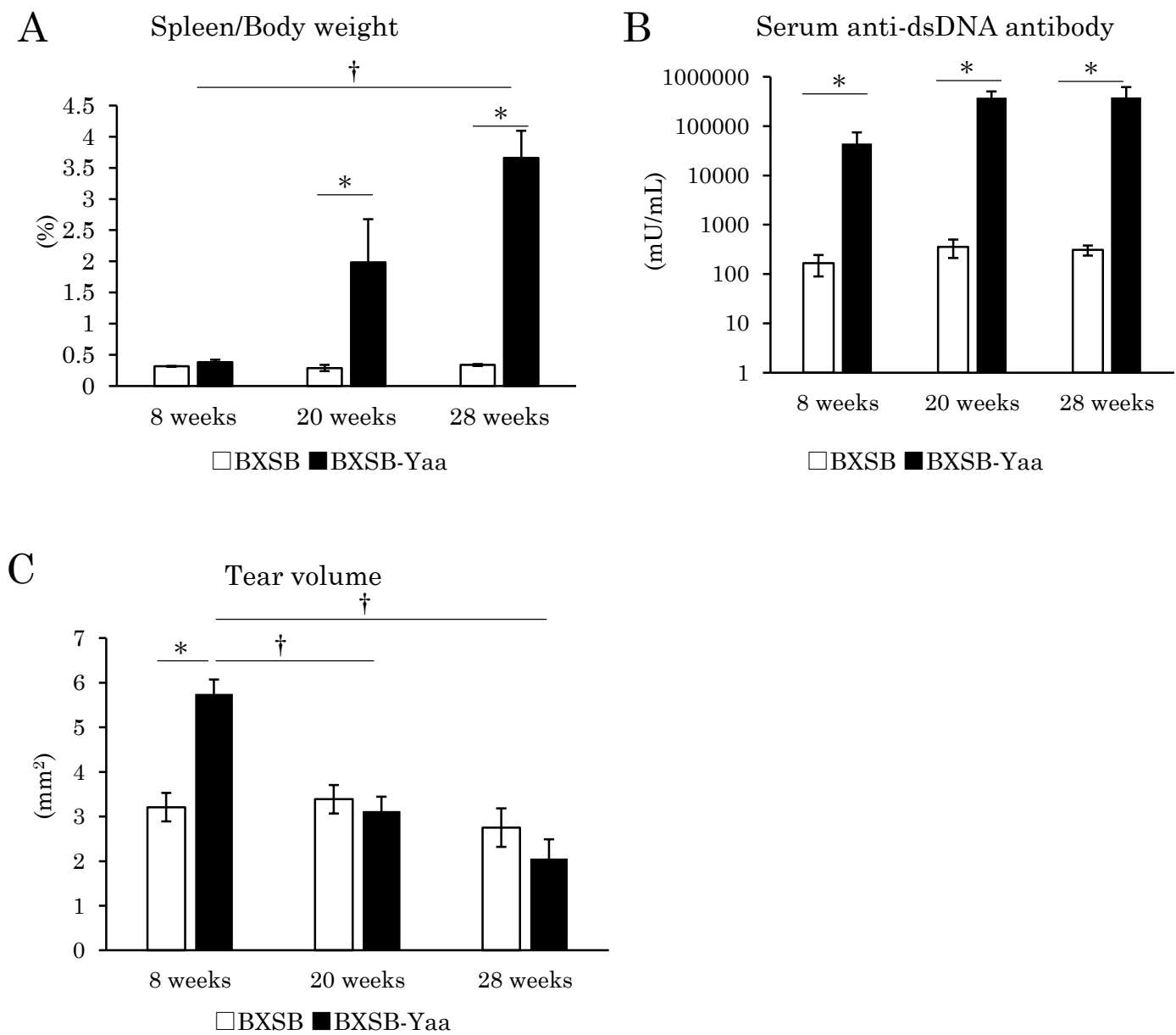
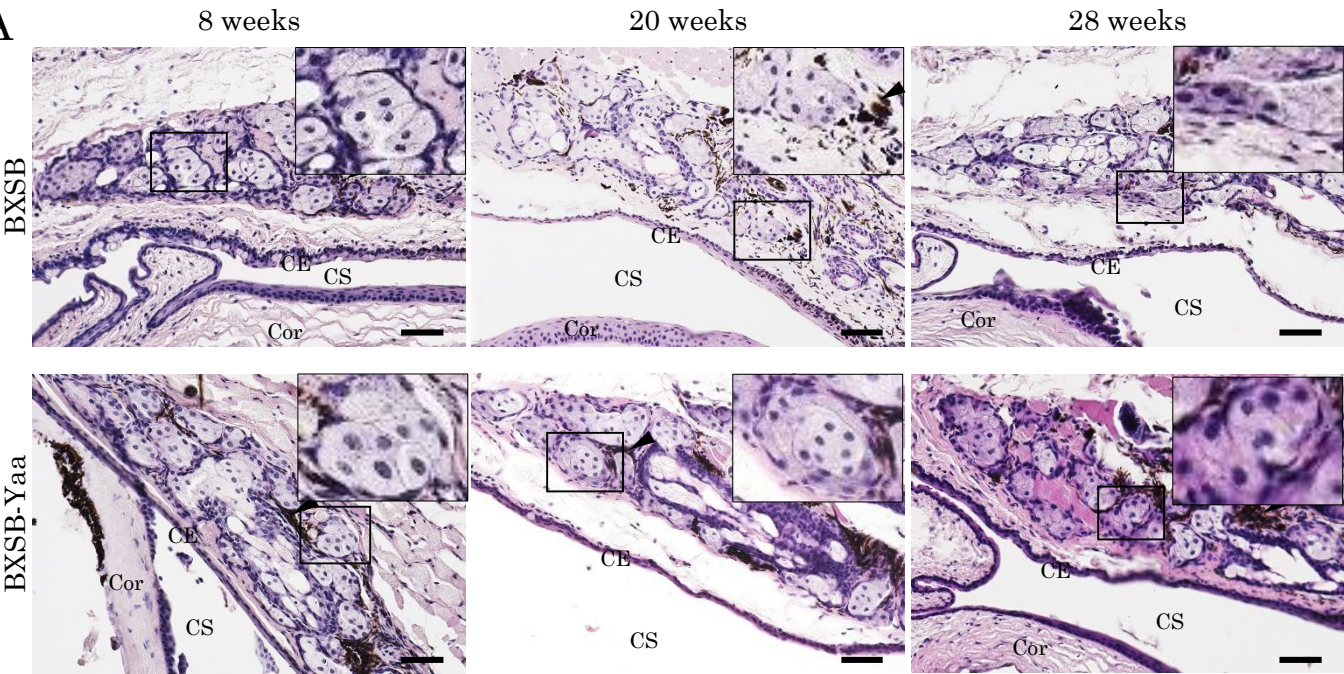
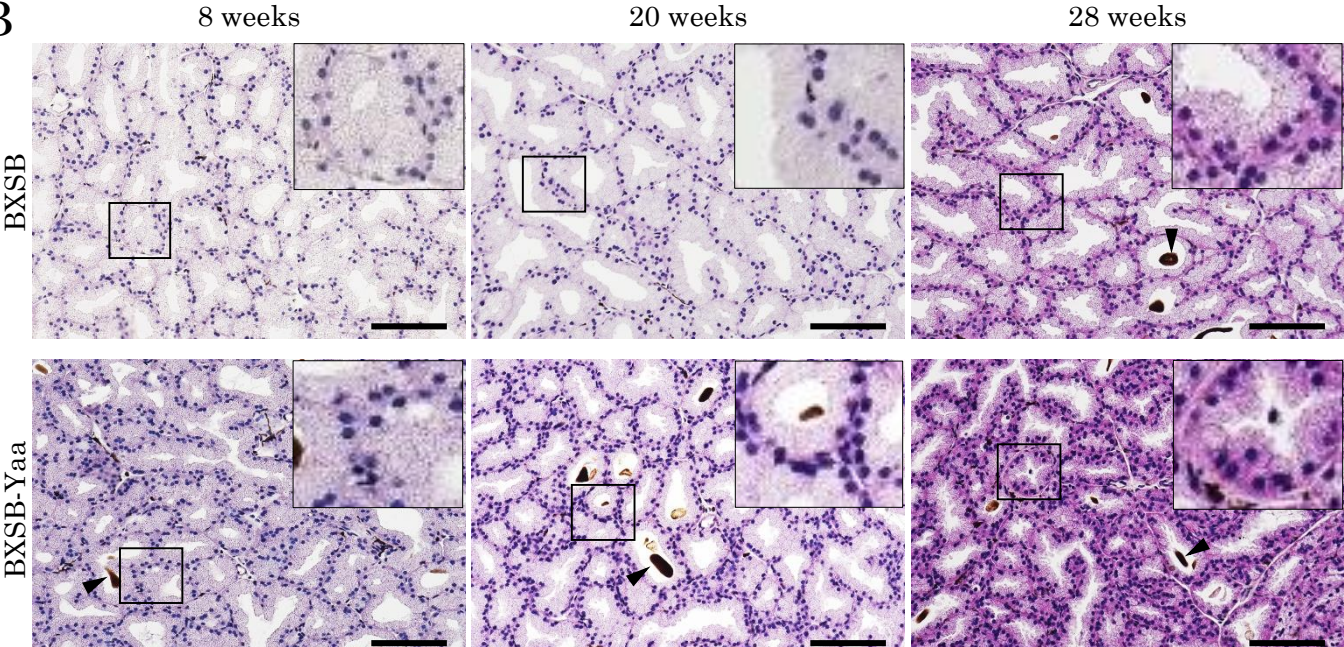


Figure. 2

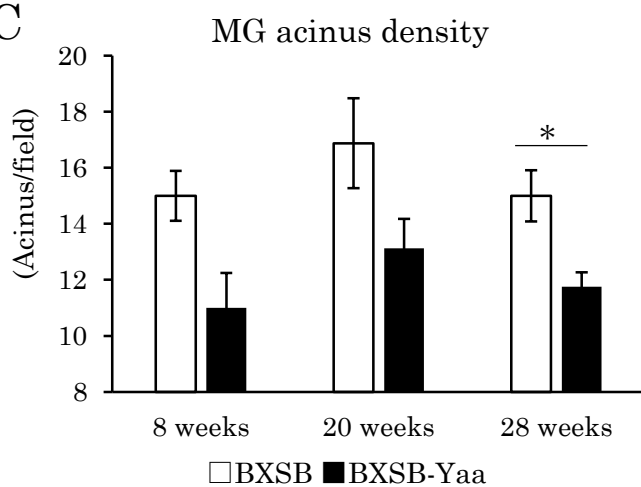
A



B



C



D

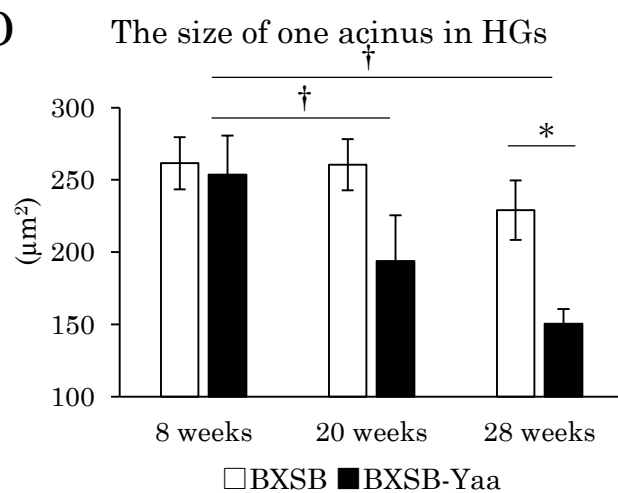
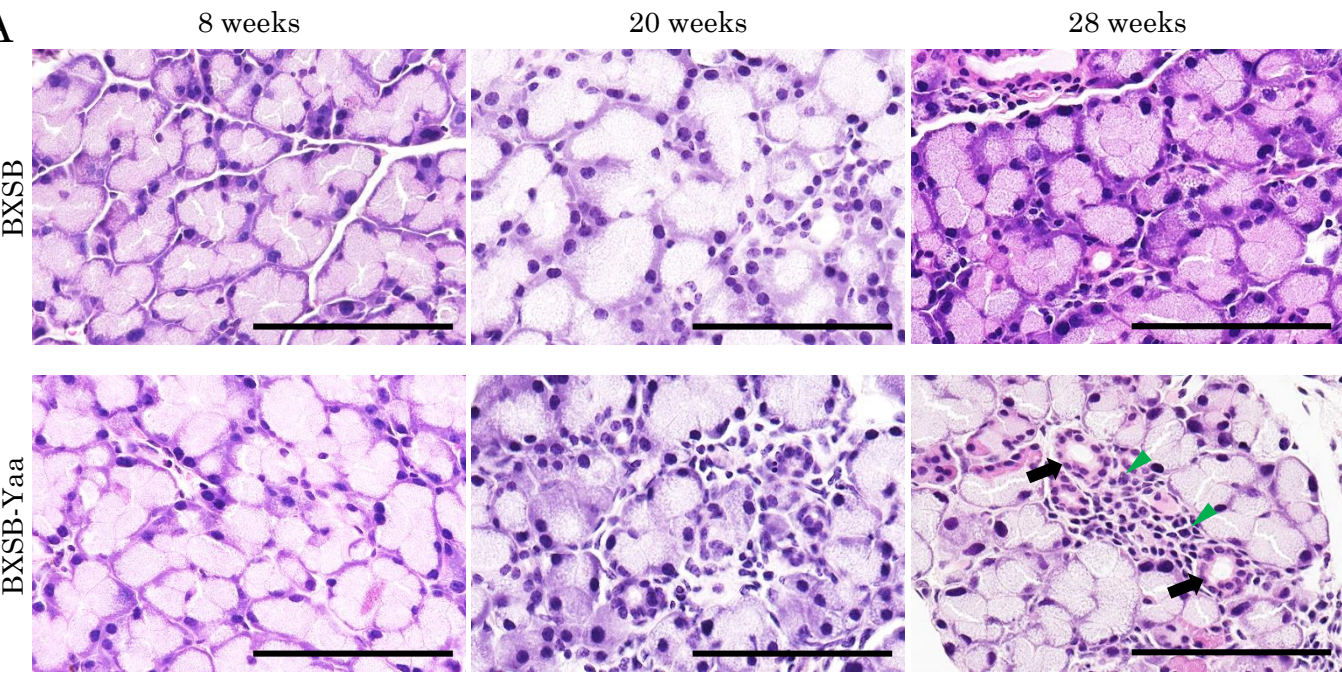
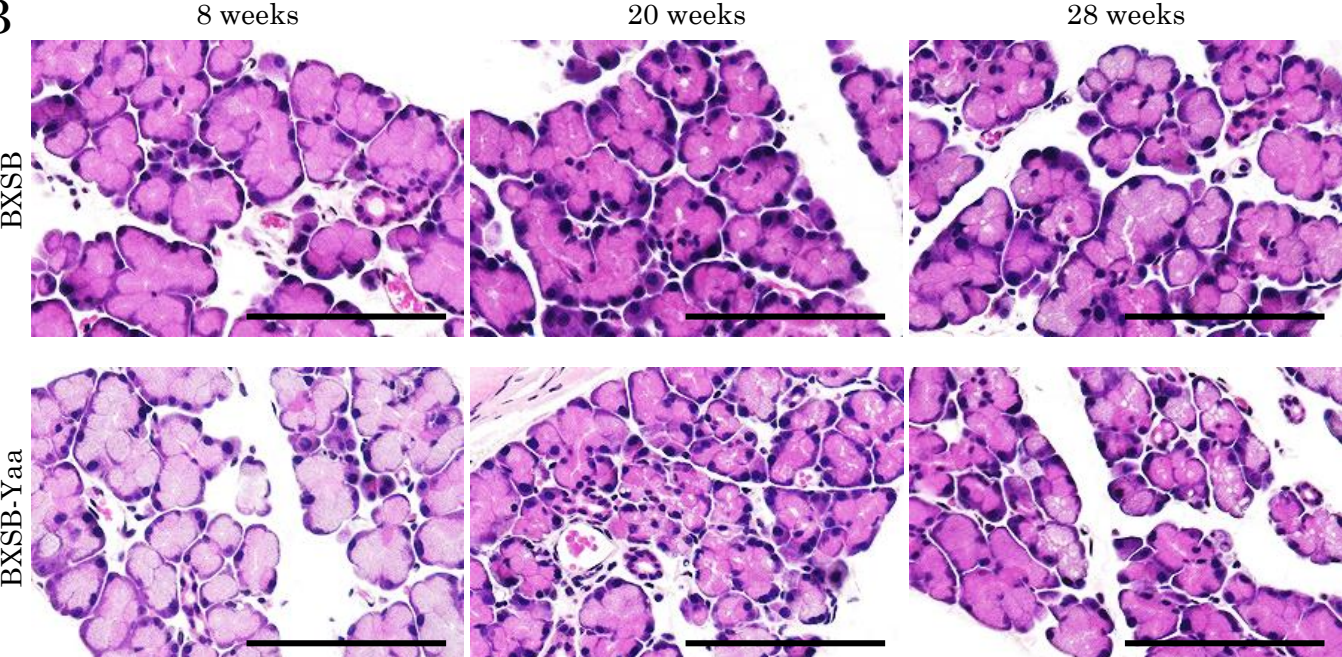


Figure. 3

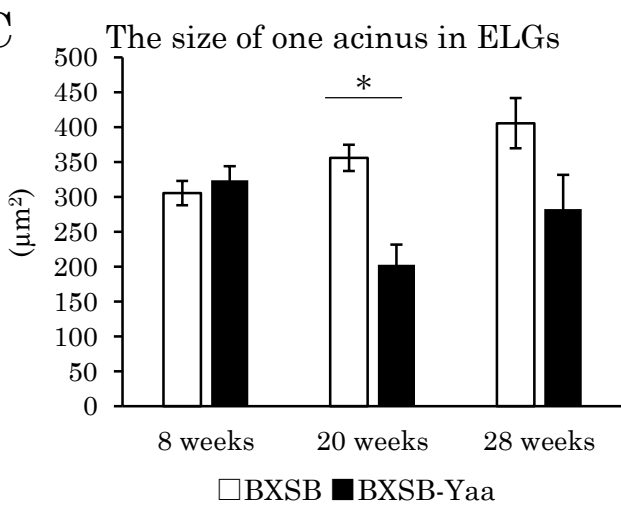
A



B



C



D

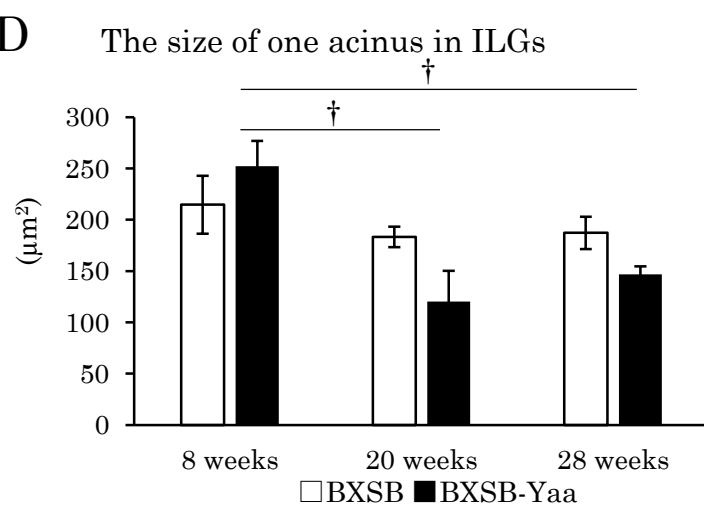


Figure. 4

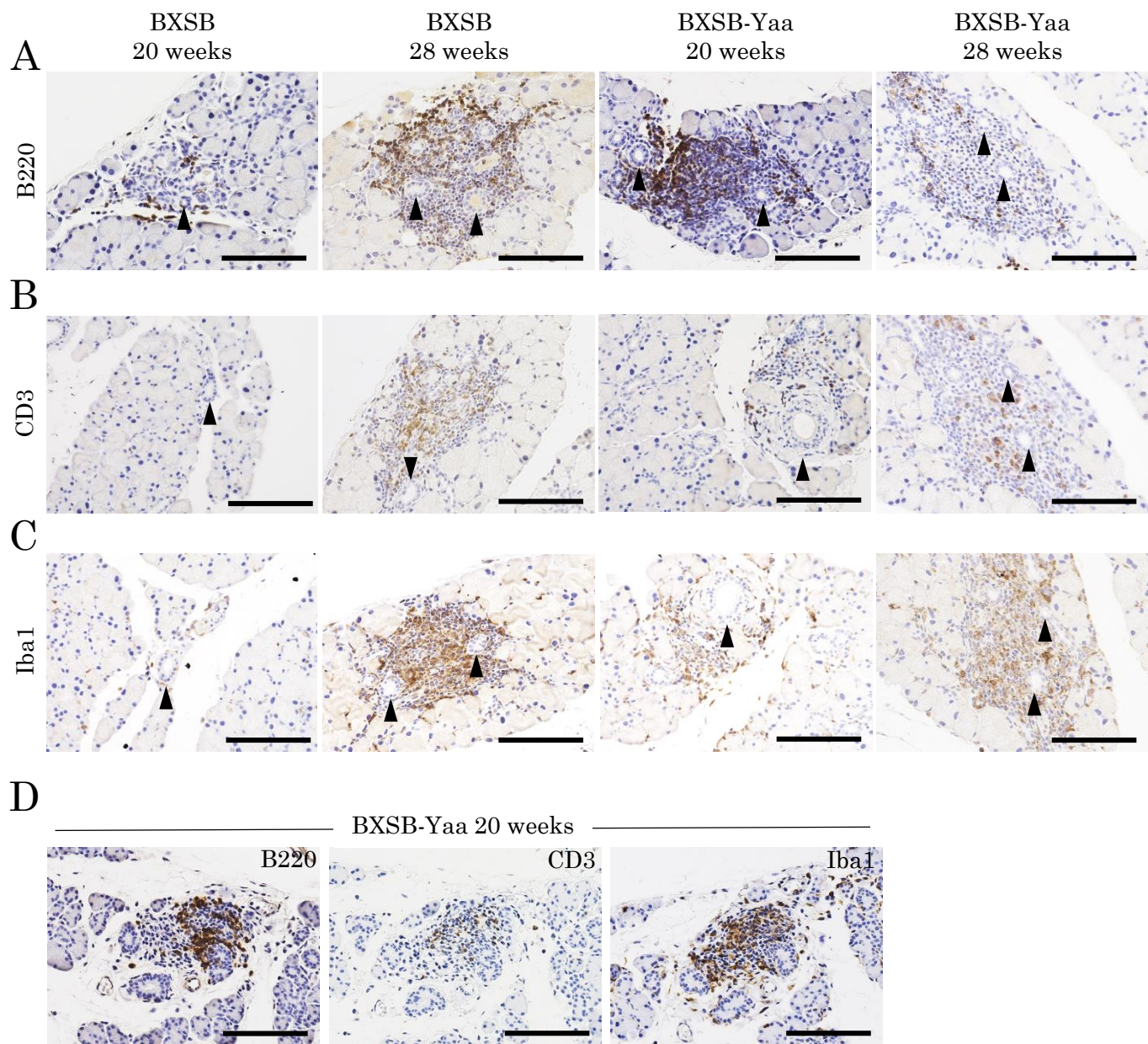
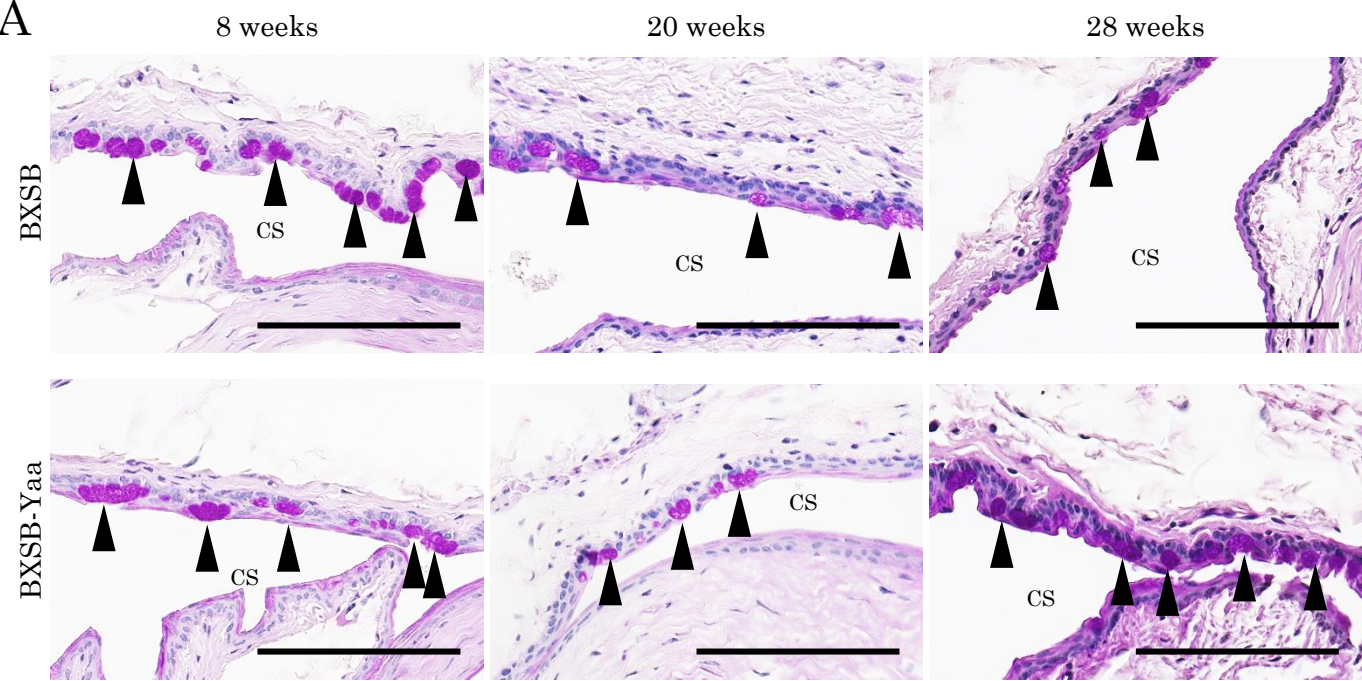


Figure. 5

A



B

Goblet cell density

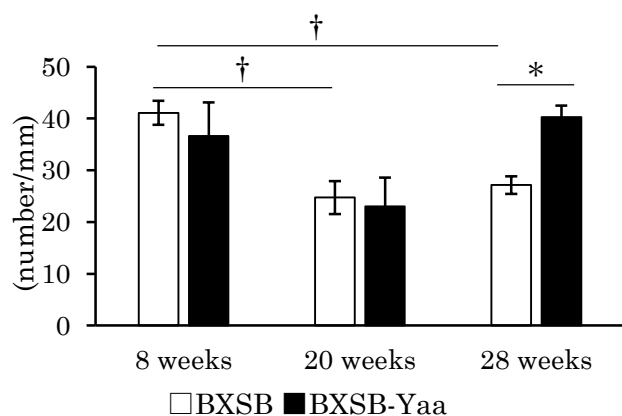
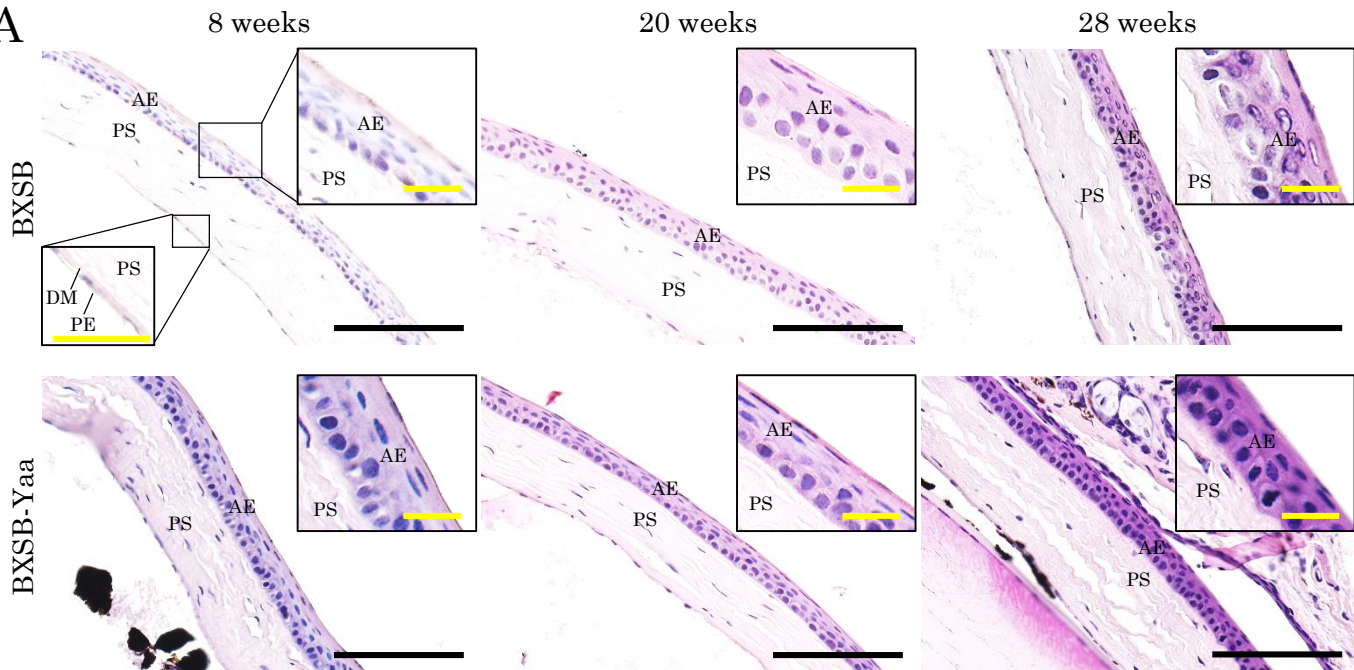
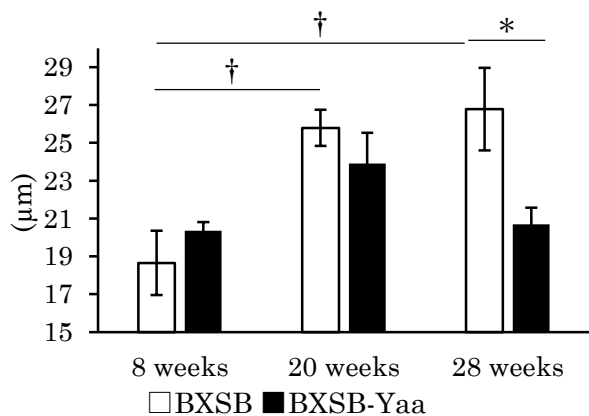


Figure. 6

A



B Thickness of cornea anterior epithelium



C

